Nat. Hazards Earth Syst. Sci. Discuss., https://doi.org/10.5194/nhess-2018-303
Manuscript under review for journal Nat. Hazards Earth Syst. Sci.
Discussion started: 30 October 2018

Natural Hazards and Earth System Sciences
Discussions

An attempt to monitor seasonal dynamics of soil salinization in the Yellow River Delta region of China using Landsat data

Hongyan Chen*, Gengxing Zhao, Yuhuan Li, Danyang Wang, Ying Ma

National Engineering Laboratory for Efficient Utilization of Soil and Fertilizer Resources, College of Resources and Environment, Shandong Agricultural University, Taian 271018, China

*Corresponding author: Hongyan Chen, College of Resources and Environment, Shandong Agricultural University, No.61 Daizong Street, Tai'an, Shandong 271018, PR China. E-mail: chenhy@sdau.edu.cn

Abstract. Monitoring seasonal dynamics of soil salinization is necessary with distinct seasonal climates. The article is to explore the optimal inversion models of soil salinity content (SSC) in different seasons and to achieve the spatial distribution and seasonal dynamics of SSC in Kenli district in the Yellow River Delta (YRD) region of China. Based on the Landsat data in 2013, the improved vegetation indices (IVI) were constucted, which were then applied in the SSC inversion model construction. Finally, the SSC optimal model in each season was extracted, then, the spatial distributions and seasonal dynamics of SSC in four seasons were analysed. The results indicated that the support vector machine (SVM) method resulted in the best inversion models. The SSC best inversion model of spring was also determined as the optimal model of winter, similarly, the best model of autumn was also as the optimal model of summer. The SSC exhibited a gradually increasing trend from the south-west to the north-east in Kenli district, and its seasonal dynamics were as that soil salinity accumulates in spring, decreases in summer, rises in autumn, and peaks in winter. This work would provide data support for the treatment and utilization of saline alkali soil in the YRD region.

Keywords: Soil salinity; Remote sensing inversion; Vegetation index; Multispectral imaging; Seasonal dynamics

Nat. Hazards Earth Syst. Sci. Discuss., https://doi.org/10.5194/nhess-2018-303
Manuscript under review for journal Nat. Hazards Earth Syst. Sci.
Discussion started: 30 October 2018

Natural Hazards and Earth System Sciences
Discussions

1. Introduction

Saline soils are widespread throughout the world, especially in arid, semi-arid and some sub-humid regions. Saline soils cause severe environmental degradation that can impede crop growth, as well as overall regional production (Metternicht and Zinck 2003; Huang et al. 2015). Obtaining soil characteristics, such as degree of salinity and geographical distribution of saline soil in real time, and improving our ability to forecast soil salinization dynamics is a necessary prerequisite for scientific management, reasonable improvement and utilization of regional saline soil (Melendez-Pastor et al. 2012). Remote sensing technologies provide an important and rapid approach for the quantitative monitoring and mapping of soil salinization (Dehni and Lounis 2012; Tayebi et al. 2013; Shoshany et al. 2013; Sidike et al. 2014; Wu et al. 2014; Guo et al. 2015; Sturari et al. 2017).

Due to the low cost and the ability to map extreme surface expressions of salinity of the imagery, multispectral satellite data, such as Landsat, System Probatoired' Observation dela Terre (SPOT), IKONOS, QuickBird, and the Indian Remote Sensing (IRS) series of satellites, have been used for mapping and monitoring of soil salinity and other properties (Dwivedi et al. 2008; Abbas et al. 2013; Allbed et al. 2014; Mahyou et al. 2016; Mehrjardi et al. 2008; Yu et al. 2010; Ahmed and Iqbal 2014; Rahmati and Hamzehpour 2016). Extensive researches have showed that models using multispectral satellite data were still the preferred method for mapping soil salinity over large spatial domains (Allbed and Kumar 2013; Scudiero et al. 2015; Taghizadeh-Mehrjardi et al. 2014). Howerver, existed researches primarily focus on SSC inversion models for a study area at a specific time (Herrero and Castañeda 2015; He et al. 2014), however, because the SSC is dynamic over time, such as through the four seasons of a year,

applying the same inversion model to analyze the SSC quantitatively in different seasons is not adequate. The Yellow River Delta (YRD) region lies within the efficient ecological economic zone of China. With nearly 550,000 ha of unused land, it has obvious geographical advantages and abundant land resources. However, soil salinization is a widespread and serious concern in this region (Mao et al. 2014). About 85.7% of the total area in the region is covered with saline soil, and there has been an increasing trend in the amount of coastal saline soil in recent years, which has seriously affected the utilization of land resources as well as the development of the regional economy and society (Yang et al. 2015; Weng et al. 2010). Moreover, the SSC in the YRD region has obvious seasonal characteristics because of the seasonal climate. Real-time, continuous monitoring of soil salinization is particularly important in this region. Seasonal SCC inversion models would greatly improve the accuracy of SSC modelling and therefore enhance our ability to monitor soil salinization of the YRD region continuously and in real-time.

The objectives of this paper are to (1) build optimal SSC inversion models for different seasons according to soil salinity condition; (2) map the spatial distribution and seasonal dynamics of SSC in the YRD region of China. Specifically, we bulit the vegetation indices by introducing the additional data of the short-wave infrared band (SWIR) available in Landsat data. The inversion models of SSC in spring and autumn were built respectively using the stepwise multiple linear regression (SMLR), back propagation neural network (BPNN) and support vector machine (SVM) methods, and the best model for spring and autumn was selected and applied to the other seasons. Once the optimal inversion model according to soil salinity was determined

for each season, it was applied for mapping the distribution of seasonal soil salinity and seasonal SSC dynamics were analyzed.

2. Materials and methods

2.1 Study area

The study area is Kenli district in the Yellow River Delta region (37°24′~38°06′N, 118°14′~119°11′E),located in Dongying city, Shandong province, China, and on the southern shore of the Bohai sea (Fig. 1).This area has characteristic plain landscape and coastal saline soil type. There are three kinds of soil subgroups: tidal soil, salinized tidal soil and coastal tidal saline soil. The soil parent material is the Yellow River alluvial material, and the soil texture is light, The levels of soil profile are obvious with salt accumulating in the soil surface while relatively little and well-distributed in the middle and lower part of the soil profile (below the core soil). The main types of land use in this area are cultivated land, unused land and grassland. The main crops are wheat, corn, rice and cotton. The main natural vegetation includes white grass, reed, horse trip grass, tamarix and suaeda. Owing to the low, flat terrain, high groundwater table, high mineralization rate, poor drainage conditions, and the infiltration and mounting of seawater associated with the Yellow River in this region, soil salinization of the surface is generally severe and widespread (Yang et al. 2015; Weng et al. 2010). With the temperate climate and four distinct seasons, soil salt content has obvious seasonal dynamics. The soil salinization process in the study area is shown in Fig. 2.

Nat. Hazards Earth Syst. Sci. Discuss., https://doi.org/10.5194/nhess-2018-303
Manuscript under review for journal Nat. Hazards Earth Syst. Sci.
Discussion started: 30 October 2018

2.2 Soil sampling and chemical analyses

To achieve an accurate representation of the seasonal climate, we selected April, August, November and February (in the following year) to represent the seasons of spring, summer, autumn, and winter, respectively. According to the climate characteristics and soil salinization conditions in the different seasons, the samples collected in spring and autumn were used to develop the inversion models of SSC, while the samples of winter and summer were used to validate the inversion models. Overall, 92 spring samples were collected during April 27~ May 2, 2013; during August 14~15, 2013, 30 summer samples were collected; 110 autumn samples were collected during November 9~ 13, 2013, and 56winter samples were collected during February 26~ 29, 2014. Sample points were designated with taking into account soil salinization degree, soil surface morphology and micro-topography, and uniformity of sample distribution (Fig. 1). Topsoil samples were collected at each sample point at a depth < 20cm and GPS coordinates were recorded. In situ environmental information was also recorded. The collected soil samples were naturally air dried, crushed, purified, passed through a 2mm sieve, and mixed evenly. The concentrations of Cl^-, SO_4^{2-}, CO_3^{2-}, HCO_3^-, K^+, Na^+, Ca^{2+}, and Mg^{2+} were measured in extracted solutions of a 1:5 soil-water mixture. The SSC was defined as the combined concentration of the eight ions mentioned above.

2.3 Acquisition and pretreatment of imaging data

Multispectral Landsat data were acquired in line with the sample collection time. We employed Landsat 7 ETM+ data of May 6, 2013, and Landsat 8 OLI data of August 18, 2013, November 6, 2013, and February 26, 2014. Landsat 7 ETM+ data include one panchromatic band (520–900 nm), four multispectral bands in the visible and near-

infrared wavelength range (blue (450–515 nm), green (525–605 nm), red (630–690 nm) and NIR (775–900 nm)), and two SWIR bands (1550–1750 nm, 2090–2350 nm). The Landsat 8 OLI data contain all of the bands of the ETM+, while the band ranges are slightly different. Image pretreatment, including geometric rectification, radiation calibration, and atmospheric correction, was conducted in ENVI 5.1 software. Geometric rectification was completed in reference to the 1:10000 terrain map of the study area, then radiation calibration and Flaash atmospheric correction were subsequently applied. The output images were projected to the Gaussain–Kruger coordinate system and cropped to the study area, then the water body, building and traffic land were masked according to the current situation of land use. Finally, the reflectance of the samples was extracted from the processed images using ArcGIS 10.1 software.

2.4 Calculation and improvement of vegetation indices

The extended vegetation indices (EVI) were all calculated based on the Landsat data by adding the SWIR band data to the traditional VI, including normalized difference vegetation index (NDVI), difference vegetation index (DVI), and ratio vegetation index (RVI) which was shown in Table 1. The correlations between SSC and EVI were analysed, then the EVI, with significant correlation coefficients, were selected as the improved vegetation indices (IVI). Finally, the IVI were used as the input to the inversion models of SSC.

Nat. Hazards Earth Syst. Sci. Discuss., https://doi.org/10.5194/nhess-2018-303
Manuscript under review for journal Nat. Hazards Earth Syst. Sci.
Discussion started: 30 October 2018

2.5 Inversion model construction and optimization

Firstly, soil samples collected in spring and autumn were sorted separately according to the SSC. Two-thirds of the samples were chosen for the calibration set, and the remaining samples were used as the validation set. So, the 92 samples of spring were divided into two groups, specifically one group of 62 samples for calibration and the other group of 30 samples for validation. Among the 110 samples of autumn, 74 samples were used for calibration, and the remaining 36 samples were used for validation. Secondly the SSC inversion model for spring was built by employing the SMLR, BPNN and SVM methods based on the VI and corresponding IVI. The performance of the SSC inversion models were evaluated by the coefficient of determination (R^2), root-mean-square error (RMSE) and ratio of performance to deviation (RPD). At the same way, the best model of SSC for autumn was built on the IVI and selected. Finally the best model for spring and autumn was respectively decided and applied to the summer and winter data, then the optimal inversion models of SSC according to soil salinization conditions in different seasons were selected.

For the SMLR method, the variance inflation factor (VIF) was set to less than 5 in order to control multicollinearity. The BPNN method was conducted using Matlab R2012a program. When calculating, the transfer function of the hidden layer and the output layer were set as tansig and logsig, respectively. The network training function was traingdx, and the learning rate, the maximum of training times, and the model expectation error were set to 0.01, 15000, and 0.01, respectively. The SVM models were built in the Libsvm 3.11 toolbox in MatlabR2012a.In this model, we selected the 4th SVM type (v-SVR) and the 2th kernel function (RBF), and the penalty parameter C

and the kernel parameter g of RBF were determined according to the minimum of mean-square deviation by using the cross-validation and grid search method.

2.6 SSC distribution mapping and year-round dynamics analysis

The reflectance spectra were extracted from the four-season Landsat data in the study area, base on which the seasonal IVI were calculated, then the SSC distribution maps of the four seasons were obtained via calculation based on the correspoding optimal models. The spatial distribution characteristics and seasonal dynamics of soil salinity in the YRD region were analysed and compared.

The methodological flow of this article is shown in Fig. 3.

3. Results

3.1 The data of soil samples

Statistical results of the samples SSC from four seasons (Table 2) showed that the SSC in the study area maintained a high level with the mean > 5.32 g/kg throughout the year. As determined from the minimum, maximum, and mean value, the SSC is highest in winter, followed by that in spring, autumn and summer, respectively. The standard deviation and coefficient of variation showed that the SSC gradient was significant overall, especially in winter and spring.

Nat. Hazards Earth Syst. Sci. Discuss., https://doi.org/10.5194/nhess-2018-303
Manuscript under review for journal Nat. Hazards Earth Syst. Sci.
Discussion started: 30 October 2018

3.2 Improved vegetation indices (IVI)

The correlation coefficients between the EVI and the SSC of the soil samples are shown in Table 3.

From Table 3, we can see that the correlation between the ERVI or EDVI and the SSC was very significant with the correlation coefficient above 0.69. So the ERVI and EDVI were selected as the IVI for spring, at the same way the ENDVI and ERVI were selected as the IVI for autumn. For each season, the chosen IVI and its corresponding VI were used to build the inversion models.

3.3 The best inversion models of SSC and its application in different seasons

3.3.1 Inversion models of SSC with VI and IVI

Results of the SSC inversion models in spring based on the IVI are shown in Table 4. In comparing the performance of three modelling methods, the prediction accuracy of the SVM models was the highest followed by the BPNN models, and the SMLR models had the lowest accuracy. In terms of the calibration values, the SVM models based on the IVI had the best and most stable inversion accuracy of SSC for both the calibration set (R^2> 0.72, RMSE <6.34 g/kg) and the validation set (R^2 > 0.71, RMSE <6.00 g/kg, and RPD >1.66), which were then selected as the best SSC inversion models of SSC in spring and autumn.

Nat. Hazards Earth Syst. Sci. Discuss., https://doi.org/10.5194/nhess-2018-303
Manuscript under review for journal Nat. Hazards Earth Syst. Sci.
Discussion started: 30 October 2018

The calibration and validation precision of SSC inversion models in spring and autumn was shown in Fig. 4.

3.3.2 Application of the best SSC inversion models with IVI in different seasons

The best *SSC* inversion models of spring and autumn were applied respectively to the SSC estimation of summer and winter. Table 5 shows the estimation accuracy. We can see that the best SSC inversion model of spring can be applied to that in winter, with R^2 of 0.66 and RMSE of 7.57g/kg. Meanwhile, the best SSC inversion model of autumn can also be applied to that in summer, resulting in $R^2$of 0.65 and RMSE of 3.60 g/kg. In response to the soil salinity condition, the SSC inversion model of spring based on IVI in combination with the SVM method was selected as the optimal SSC model for spring and winter, while the SSC inversion model of autumn based on IVI in combination with the SVM method was selected as the optimal SSC model for autumn and summer in the YRD region.

3.4 Distribution and seasonal dynamics of SSC in the Yellow River Delta region

3.4.1 Distribution of SSC in four seasons

Based on the processed Landsat data and the optimal SSC inversion models for each season, the inversion maps of SSC in the four seasons were obtained. The descriptive statistics of the inversed SSC in four seasons are shown in Table 6, which are close to those of the collected samples (Table 2); the inversion results also showed that the SSC in winter was highest, followed by that in spring, and the SSC in autumn and summer were relatively low.

Nat. Hazards Earth Syst. Sci. Discuss., https://doi.org/10.5194/nhess-2018-303
Manuscript under review for journal Nat. Hazards Earth Syst. Sci.
Discussion started: 30 October 2018

According to the classification standard of coastal saline soil in the semi-humid area of China, the study area was divided into 5 grades of soil salinization. The distribution of soil salinity grades in the four seasons were mapped (Fig. 5). The spatial distributions of SSC in the four seasons showed similar characteristics. There was a gradually increasing trend of soil salinity from the south-west to the north-east part of the study region, and this distribution pattern is consistent with the results of other studies (Weng et al. 2010; Yang et al. 2015). The main reason for this gradual increase of SSC is that the terrain of the south-west part of the study area is high and flat, with the flood-prone land used for agricultural production. The central part of the region, near the banks of the Yellow River, has alternate hillocks, slopes and depressions, which was formed by the repeated diversion of the Yellow River; thus, each grade of soil salinization was also alternately distributed, and the north-east part of the region which has low terrain and is closest to the sea, has the most severe soil salinization.

3.4.2 Seasonal dynamics of SSC

The number of pixels and proportion of pixels per SSC grade were calculated for each season (Table 7). Fig. 5 and Table 7 demonstrated that the SSC in the study area is clearly different among the four seasons. The SSC in spring consisted primarily of moderately saline soil, severely saline soil, and solonchak (combined proportion of 90.05%); in summer, the area of the four grades from the mildly saline soil to solonchak was relatively uniform (each grade accounting for 22 – 28%); the SSC during autumn was largely dominated by severely saline soil and solonchak (combined proportion of 77.75%); in winter, the SSC was principally severely saline and solonchak, with the combined proportion of 99.19%, of which the severe saline soil contributed 80.71% .

Nat. Hazards Earth Syst. Sci. Discuss., https://doi.org/10.5194/nhess-2018-303
Manuscript under review for journal Nat. Hazards Earth Syst. Sci.
Discussion started: 30 October 2018

The seasonal SSC inversion values and the proportion of pixels per SSC grade indicated that the change of SSC between different seasons is relatively apparent. The degree of soil salinization was lowest in summer, and the SSC in autumn was relatively low except for the solonchak in coastal areas. In spring, the soil salinization became more obvious, with most of the study area belonging to the moderate to severe saline soil and solonchak group. Meanwhile the soil salinization was the most severe in winter. In summary, soil salinity in the study area usually accumulates in spring, decreases in summer, rises in autumn, and peaks in winter.

4. Discussion

We can see that the best SSC inversion models of spring and autumn are based on different IVI. In spring, the weather is characteristically drought, windy, and strong evaporated, and the coverage of natural vegetation is low; however, crops such as wheat and corn are in a vigorous growth stage, which results in strong reflectance spectra of vegetation. Generally, RVI and DVI are sensitive to vegetation especially when vegetation coverage is high, thus the inversion accuracy based on ERVI and EDVI is higher than that of other vegetation indices. In autumn, rainfall and temperature are reduced, and there is little coverage of natural vegetation, cotton has been collected with only withered cotton leaves and rods leaved in the field, and wheat has just drilled out of the soil. Therefore, the reflectance spectra of vegetation are relatively weak. NDVI has low sensitivity to high vegetation areas and is suitable for monitoring in low and moderate vegetation coverage areas, so the inversion accuracy based on ENDVI and ERVI is higher than that of the other vegetation indices. The results were obtained

without considering some factors (e.g. soil moisture and temperature) that vary with seasons and affect SSC, the influence of some key factors will be studied to remove in the future study.

The seasonal dynamics of SSC are closely related to the climate of the study area. With drought, windy weather, and strong evaporation in spring from March to May, soil salts aggregate to the soil surface as soil moisture goes up, which form the first peak of salt accumulation, with the total 90.05% of moderately saline soil, severely saline soil, and solonchak. Rainfall and floods occur in the summer from June to August and as precipitation infiltrates into the soil, the soil surface is desalinated, with uniform proportion from the mildly saline soil to solonchak. In the autumn from September to November, rainfall reduces and SSC increases slightly, with largely dominated by severely saline soil and solonchak (combined proportion of 77.75%). Due to drought in winter from December to February, combined with less evaporation than in spring, soil salinization is relatively severe and remains latent in the surface soil, with the 99.19% of severely saline and solonchak. By the end of the season, the salt will rise to the peak.

The article aimed to build optimal SSC inversion models for different seasons according to soil salinity condition in one year, and the SSC at the point of time was used as the corresponding seasonal salt data. The results indicated that the SSC inversion model of spring could be applied in winter resulting in R^2 of 0.66 and RMSE of 7.57 g/kg, while the SSC inversion model of autumn could also be applied in summer resulting in R^2 of 0.65 and RMSE of 3.60 g/kg within a year in the YRD region. This model selection results may be due to the short time intervals and similar soil salt

climatic conditions between February and April and between August and November in the Yellow River Delta region. In order to respond more accurately to the dynamic changes of soil salt, a period of SSC should be selected as the seasonal salt data, which will be the future research, and the application of the SSC inversion models for different years will be explored.

5. Conclusion

In this experiment, the results showed that the extended ratio vegetation index (ERVI) and extended difference vegetation index (EDVI) were as IVI of spring, while the extended normalized difference vegetation index (ENDVI) and extended ratio vegetation index (ERVI) were as the IVI of autumn. The best and most stable accuracy of SSC was produced by the SVM models based on the IVI; therefore, these models were selected as the best SCC inversion models of spring and autumn. The experiment results would contribute to the quantitative and accurate monitoring of soil salinization with multispectral imaging.

This experiment indicates that the best inversion model of spring could be applied for the SSC inversion of winter and was selected as the optimal SSC model of spring and winter in response to soil salinity condition; at the same time, the best inversion model of autumn could also be applied to the SSC inversion of summer and was selected as the optimal SSC model of autumn and summer in the Yellow River Delta region.

The SSC spatial distribution of each season in the study area was determined using the SCC inversion model optimized for each season. In the Yellow River Delta region, the spatial distribution of SSC shows a gradually increasing trend from the south-west to the north-east. The seasonal dynamics of SSC are such that soil salts accumulate in spring, decrease in summer, rise in autumn, and peak in winter.

Author contributions. Hongyan Chen analyzed the data and prepared the manuscript. Gengxing Zhao developed the framework for the study. Danyang Wang and Ying Ma collected and analyzed the data. Yuhuan Li provided technical support throughout different stages of the study. All coauthors provided manuscript review.

Competing interests. The authors declare that they have no conflict of interest.

Acknowledgments

This work was financially supported by the National Natural Science Foundation of China; under Grant(number 41877003 and 41671346); the National Science and Technology Support Program of China; under Grant (number 2015BAD23B0202); the Funds of Shandong “Double Tops” Program; under Grant (number SYL2017XTTD02); and Shandong Province key R & D Plan of China; under Grant(number 2017CXGC0306).

References

Abbas, A., Khan, S., Hussain, N., Hanjra, M. A., and Akbar, S.: Characterizing Soil Salinity in Irrigated Agriculture using A Remote Sensing Approach. Physics and Chemistry of the Earth Parts, A/B/C55–57, 43–52. doi: 10.1016/j.pce.2010.12.004, 2013.

Ahmed, Z., and Iqbal, J.: Evaluation of Landsat TM5 Multispectral Data for Automated Mapping of Surface Soil Texture and Organic Matter in GIS. European Journal of Remote Sensing, 47(1), 557-573. doi: 10.5721/EuJRS20144731, 2014.

Allbed, A., Kumar, L., and Aldakheel, Y.Y.: Assessing Soil Salinity using Soil Salinity and Vegetation Indices derived from IKONOS High-spatial Resolution Imageries Applications in A Date Palm Dominated Region. Geoderma, 230–231, 1–8. doi: 10.1016/j.geoderma.2014.03.025, 2014.

Allbed, A., and Kumar. L.: Soil Salinity Mapping and Monitoring in Arid and Semi-arid Regions using Remote Sensing Technology: A Review. Advances in Remote Sensing, 2, 373–385. doi: 10.4236/ars.2013.24040, 2013.

Dehni, A., and Lounis. M.: Remote Sensing Techniques for Salt Affected Soil Mapping: Application to the Oran Region of Algeria. Procedia Engineering, 33, 188–198. doi: 10.1016/j.proeng.2012.01.1193, 2012.

Dwivedi, R.S., Kothapalli, R.V., and Singh. A. N.: Generation of Farm-level Information on Salt-affected Soils using IKONOS-II Multispectral Data. Remote Sensing of Soil Salinization: Impact on Land Management. CRC Press, Taylor and Francis, New York, 73–89. doi: 10.1201/9781420065039.ch5, 2008.

Guo, Y., Shi, Z., Zhou, L. Q., Jin, X., Tian, Y. F., and Teng. H. F.: Integrating Remote Sensing and Proximal Sensors for the Detection of Soil Moisture and Salinity Variability in Coastal Areas. Journal of Integrative Agriculture, 12, 723–731. doi: 10.1016/S2095-3119(13)60290-7, 2013.

He, B., Cai, Y.L., Ran, W.R.,and Jiang. H.: Spatial and Seasonal Variations of Soil Salinity following Vegetation Restoration in Coastal Saline Land in Eastern China. Catena, 118, 147–153. doi: 10.1016/j.catena.2014.02.007, 2014.

Herrero, J., andCastañeda. C.: Temporal Changes in Soil Salinity at Four Saline Wetlands in NE Spain. Catena, 133, 145–156. doi: 10.1016/j.catena.2015.04.017, 2015.

Huang, J. Y., Shi, Z., and Biswas. A.: Characterizing Anisotropic Scale-specific Variations in Soil Salinity from A Reclaimed Marshland in China. Catena, 131, 64–73. doi: 10.1016/j.catena.2015.04.017, 2015.

Mahyou, H., Tychon, B., Balaghi, R., Louhaichi, M., and Mimouni. J.: A Knowledge-based Approach for Mapping Land Degradation in the Arid Rangelands of North

Africa. Land Degradation & Development, 27, 1574–1585. doi: 10.1002/ldr.2470, 2016.

Mao, W. B., Kang, S. Z., Wan, Y. S., Sun, Y. X., Li, X. H., and Wang. Y. F.: Yellow River Sediment as A Soil Amendment for Amelioration of Saline Land in the Yellow River Delta. Land Degradation & Development, 27, 1595–1602. doi: 10.1002/ldr.2323, 2014.

Mehrjardi, R. T., Mahmoodi, S., Taze, M.,and Sahebjalal. E.: Accuracy Assessment of Soil Salinity Map in Yazd-Ar-dakan Plain, Central Iran, based on Landsat ETM+ Imagery. American-Eurasian Journal of Agricultural & Environmental Sciences, 3, 708–712, 2008.

Melendez-Pastor, I., Hernández, E. I., Navarro-Pedreño, J., and Gomez. I.: Mapping Soil Salinization of Agricultural Coastal Areas in Southeast Spain. Remote Sensing Applications, 6, 117–140.doi: 10.5772/36805, 2012.

Metternicht, G. I., and Zinck. J.A.: Remote Sensing of Soil Salinity: Potentials and Constraints. Remote Sensing of Environment, 85, 1–20.doi: 10.1016/S0034-4257(02)00188-8, 2003.

Rahmati, M., and Hamzehpour. N.: Quantitative Remote Sensing of Soil Electrical Conductivity using ETM+ and Ground Measured Data. International Journal of Remote Sensing, 38 (1), 123–140. doi: 10.1080/01431161.2016.1259681, 2016.

Scudiero, E., T. H. Skaggs, and D. L. Corwin.: Regional-scale Soil Salinity Assessment using Landsat ETM + canopy Reflectance. Remote Sensing of Environment, 169, 335–343. doi: 10.1016/j.rse.2015.08.026, 2015.

Shoshany, M., Goldshleger, N., and Chudnovsky. A.: Monitoring of Agricultural Soil Degradation by Remote-sensing Methods: A Review. International Journal of Remote Sensing, 34 (17), 6152–6181. doi: 10.1080/01431161.2013.793872, 2013.

Sidike, A., Zhao, S. H., and Wen. Y.M.: Estimating Soil Salinity in Pingluo County of China using Quick Bird Data and Soil Reflectance Spectra. International Journal of Applied Earth Observation and Geoinformation, 26, 156–175. doi: 10.1016/j.jag.2013.06.002, 2014.

Sturari, M., Frontoni, E., Pierdicca, R., Mancini, A., Malinverni, E. S., Tassetti, A. N., and Zingaretti, P.: Integrating Elevation Data and Multispectral High-resolution Images for an Improved Hybrid Land Use/Land Cover Mapping. European

Journal of Remote Sensing, 50(1), 1-17. doi: 10.1080/22797254.2017.1274572, 2017.

Taghizadeh-Mehrjardi, R., Minasny, B., Sarmadian, F.,and Malone. B.: Digital Mapping of Soil Salinity in Ardakan Region, Central Iran. Geoderma, 213, 15–28. doi: 10.1016/j.geoderma.2013.07.020, 2014.

Tayebi, M. H., Tangestani, M. H., and Hasan Roosta. M. H.: Mapping Salt Diapirs and Salt Diapir-affected Areas using MLP Neural Network Model and ASTER Data. International Journal of Digital Earth, 6, 143-157. doi: 10.1080/17538947.2011.606336, 2013.

Weng, Y. L., Gong, P.,and Zhu. Z. L.: A Spectra Index for Estimating Soil Salinity in the Yellow River Delta region of China using EO-1 Hyperion Data. Pedosphere, 20, 378–388. doi: 10.1016/S1002-0160(10)60027-6, 2010.

Wu, W. C., Mhaimeed, A.S., Al-Shafie, W.M., Ziadat, F., Dhehibi, B., Nangia, V., and Pauw. E. D.: Mapping Soil Salinity Changes using Remote Sensing in Central Iraq. Geoderma Regional, 2–3, 21–31. doi: 10.1016/j.geodrs.2014.09.002, 2014.

Yang, L., Huang, C., Liu, G.C., Liu, J., and Zhu. A. X.: Mapping Soil Salinity using A Similarity-based Prediction Approach: A Case Study in Yellow River Delta, China. Chinese Geographical Science, 25, 283–294.doi: 10.1007/s11769-015-0740-7, 2015.

Yu, R., Liu, T. X., Xu, Y. P., Zhu, C., Zhang, Q., Qu, Z.Y., Liu, X.M., and Li. C.Y.: Analysis of Salinization Dynamics by Remote Sensing in Hetao Irrigation District of North China. Agricultural Water Management, 97, 1952–1960.doi: 10.1016/j.agwat.2010.03.009, 2010.

Nat. Hazards Earth Syst. Sci. Discuss., https://doi.org/10.5194/nhess-2018-303
Manuscript under review for journal Nat. Hazards Earth Syst. Sci.
Discussion started: 30 October 2018

Natural Hazards and Earth System Sciences
Discussions

Tables

Table 1. Calculation of extended vegetation indices

Extended vegetation indices (EVI)	Calculation formula
Extended normalized difference vegetation index (ENDVI)	(*NIR*+*SWIR*-*R*)/(*NIR*+*SWIR*+*R*)
Extended ratio vegetation index (ERVI)	(*NIR*+*SWIR*)/*R*
Extended difference vegetation index (EDVI)	*NIR*+*SWIR*-*R*

Note: the SWIR band refers to either of the two SWIR bands.

Table 2. Descriptive statistics of the soil sample SSC

Seasons	Minimum (g/kg)	Maximum (g/kg)	Mean (g/kg)	Standard deviation (g/kg)	Coefficient of variation	Sample points
Spring	1.10	46.70	8.60	11.50	1.34	92
Summer	1.34	29.20	5.32	5.95	1.12	30
Autumn	0.90	36.70	7.80	8.20	1.05	110
Winter	2.00	61.50	9.50	12.00	1.26	56

Table 3. Correlation analysis between vegetation indices and SSC

Correlation coefficients	Extended vegetation indices		
	ENDVI	ERVI	EDVI
Spring	-0.52**	-0.69**	-0.70**
Autumn	-0.73**	-0.69**	-0.69**

Significance levels: [**] 0.01

Nat. Hazards Earth Syst. Sci. Discuss., https://doi.org/10.5194/nhess-2018-303
Manuscript under review for journal Nat. Hazards Earth Syst. Sci.
Discussion started: 30 October 2018

Natural Hazards and Earth System Sciences
Discussions

Table 4. Inversion models of SSC with IVI from Landsat data

Modelling methods	Spring					Autumn				
	Calibration set		Validation set			Calibration set		Validation set		
	R^2	RMSE (g/kg)	R^2	RMSE (g/kg)	*RPD*	R^2	RMSE (g/kg)	R^2	RMSE (g/kg)	*RPD*
SMLR	0.42	9.03	0.62**	6.83	1.36	0.65**	3.42	0.56	3.81	2.01
BPNN	0.60**	7.56	0.57**	7.30	1.47	0.72**	3.39	0.68**	3.38	2.15
SVM	0.72**	6.34	0.71**	6.00	1.66	0.75**	3.48	0.78**	3.02	2.56

Significance levels: [**] 0.01

Table 5. Application of the best SSC inversion models

	The best inversion model of spring		The best inversion model of autumn	
	R^2	RMSE (g/kg)	R^2	RMSE (g/kg)
Summer samples (30)	0.23	5.31	0.65**	3.60
Winter samples (56)	0.66**	7.57	0.28	10.98

Significance levels: [**] 0.01

Table 6. Descriptive statistics of the inversion SSC

	Minimum (g/kg)	Maximum (g/kg)	Mean (g/kg)	Standard deviation (g/kg)
Spring	0.86	53.44	8.79	10.26
Summer	1.00	35.50	7.00	4.18
Autumn	0.82	35.15	8.28	9.21
Winter	1.12	58.10	9.21	13.78

Nat. Hazards Earth Syst. Sci. Discuss., https://doi.org/10.5194/nhess-2018-303
Manuscript under review for journal Nat. Hazards Earth Syst. Sci.
Discussion started: 30 October 2018

Natural Hazards and Earth System Sciences
Discussions

Table 7. The pixels number and proportion of pixels per SSC grade in four seasons

Grades	Spring		Summer		Autumn		Winter	
	Pixel number	Proportion%	Pixel number	Proportion%	Pixel number	Proportion%	Pixel number	Proportion%
Non-saline soil (<2.0 g/kg)	10705	0.67	16	0	46439	2.89	3	0
Mild saline soil (2.0~4.0 g/kg)	84805	5.29	450331	28.07	127262	7.93	12	0
Moderate saline soil(4.0~6.0 g/kg)	451291	28.13	427216	26.63	182589	11.37	13045	0.81
Severe saline soil(6.0~10.0 g/kg)	597607	37.25	371641	23.16	305762	19.05	1294867	80.71
Solonchak (>10.0 g/kg)	459989	28.67	355193	22.14	942345	58.70	296470	18.48

Figures

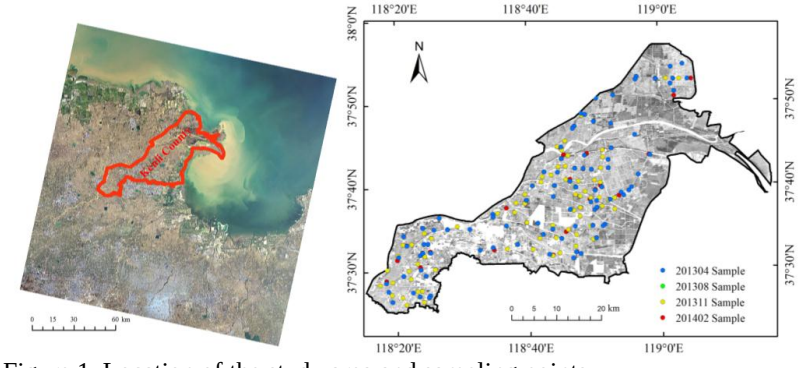

Figure 1. Location of the study area and sampling points

Nat. Hazards Earth Syst. Sci. Discuss., https://doi.org/10.5194/nhess-2018-303
Manuscript under review for journal Nat. Hazards Earth Syst. Sci.
Discussion started: 30 October 2018

Natural Hazards and Earth System Sciences
Discussions

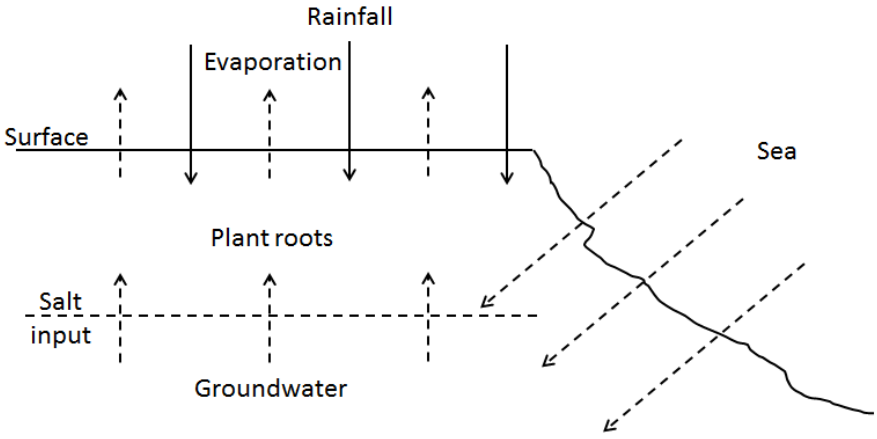

Figure 2. Soil salinization process in the study area

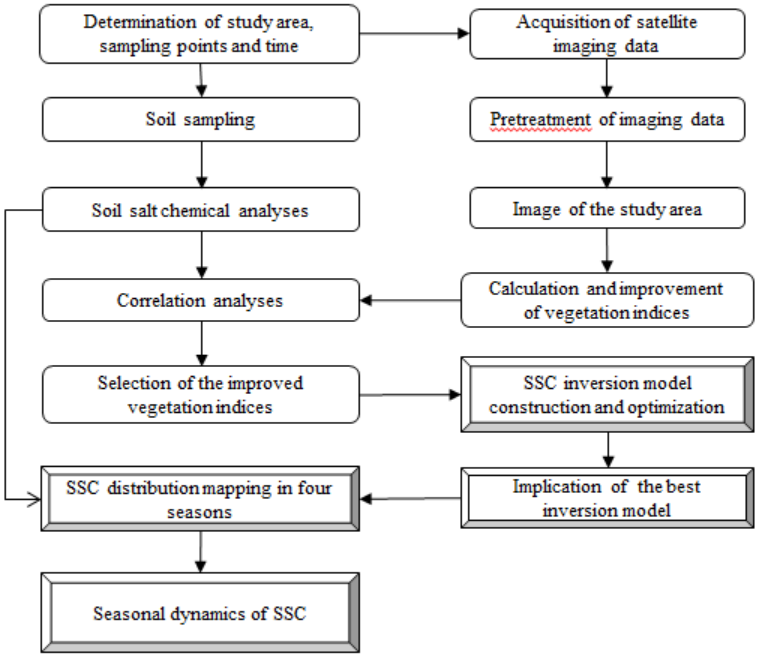

Figure 3. The methodological flow-chart

Nat. Hazards Earth Syst. Sci. Discuss., https://doi.org/10.5194/nhess-2018-303
Manuscript under review for journal Nat. Hazards Earth Syst. Sci.
Discussion started: 30 October 2018

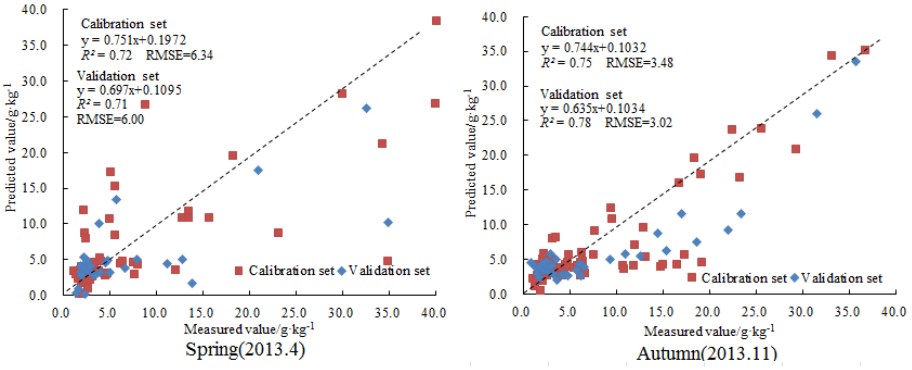

Figure 4. The calibration and validation precision of SSC inversion models in spring and autumn

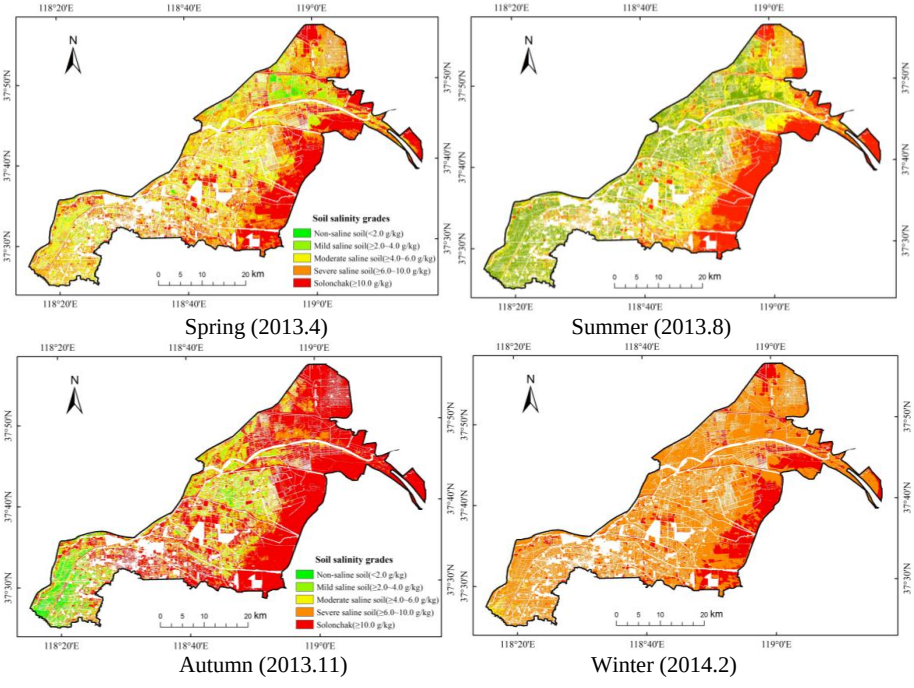

Figure 5. The inversion and distribution of SSC in four seasons